Morse Stretch Potential Charge Equilibrium Force Field for Ceramics: Application to the Quartz-Stishovite Phase Transition and to Silica Glass

Ersan Demiralp,* Tahir Çağin,† and William A. Goddard III‡

Materials and Process Simulation Center, Beckman Institute (139-74), Division of Chemistry and Chemical Engineering, California Institute of Technology, Pasadena, California 91125

(Received 7 July 1998)

To predict phase transitions in ceramics and minerals from molecular dynamics simulations, we have developed a force field in which the charges are allowed to readjust instantaneously to the atomic configurations. These charges are calculated using the charge equilibration (QEq) method. In addition to electrostatics, a two-body Morse stretch potential is included to account for short-range nonelectrostatic interactions. This MS-Q potential is applied herein to SiO_2, where we find that it describes well the fourfold coordinated and sixfold coordinated systems (such as quartz and stishovite), silica glass, and the pressure-induced phase transition from quartz to stishovite. [S0031-9007(99)08499-9]

PACS numbers: 62.50.+p, 61.43.Fs, 64.70.Kb

In principle, the phase transitions in minerals and ceramics can be predicted from first principles quantum mechanics (QM), and significant progress is being made along this line [1–3]. However, most QM studies have considered only static conditions since dynamical QM simulations are usually not practical for long times (at least nanoseconds) and large system sizes of interest for ceramics. Thus, we need to use classical molecular dynamics (MD) for predicting such phenomena. The problem here is that standard approaches to force fields (FF) [4–7] for ceramics and oxides use simplifications (fixed charges, three-body potentials) or valence terms [8] which may not be appropriate for describing phase transitions, where the ligancy and structure may change dramatically. For this reason, we have developed an alternative procedure more likely to describe phase transitions of ceramics. Herein we outline the methodology and report the first results for SiO_2 systems.

Because electrostatics play an essential role in determining the structure and properties of ceramics, we consider that the first priority of the FF is to produce plausible charges. Since the charges may depend on the distances, angles, and ligancy, we consider that *the charge must be allowed to readjust to the instantaneous configuration of the atoms.* To do this we use the charge equilibration (QEq) procedure developed by Rappé and Goddard [9] and used in many applications on organic and inorganic systems [10]. Rather than keeping the charges fixed during the dynamics, as in previous calculations, we now allow the charges to adjust to the instantaneous geometric configuration of the atoms.

In QEq the charges are determined by requiring that the chemical potential χ_A be equal on all atoms, and χ_A is a function of the charges on all of the atoms of the system:

$$\chi_A(Q_1, \ldots, Q_N) = \chi_A^0 + \sum_B J_{AB}(R_{AB}) Q_B \,. \qquad (1)$$

Here, the atomic parameters χ_A^0 and J_{AA}^0 correspond physically to the electronegativity and hardness of the atom and are obtained from the valence-averaged atomic ionization potential (IP) and electron affinity (EA) as $\chi_A^0 = (IP_A - EA_A)/2$ and $J_{AA}^0 = (IP_A + EA_A)$. $J_{AB}(R)$ is described as a shielded Coulomb potential for a normalized ns Slater orbital, $\Phi_{n\zeta}^{\text{stat}} = N_n r^{n-1} e^{-\zeta r}$, where the orbital exponent ζ_{AB} is given by $\zeta_{AB}^{-1} = (R_A/n_A + R_B/n_B)$, and R_A is the radius of the atom in the standard state ($R_{\text{Si}} = 1.176$ Å and $R_{\text{O}} = 0.669$ Å). The asymptotic limits of J_{AB} (R_{AB}) are

$$J_{AB}(R) = \begin{cases} 1/R & \text{as } R \to \infty \\ J_0 & \text{as } R \to 0 \end{cases} . \qquad (2)$$

Thus, J_{AB} describes simple Coulomb for large separations, but it is shielded for short distances. The QEq parameters used for Si and O are given in Table Ib [9].

The nonelectrostatic interactions (short-range Pauli repulsion, covalency, dispersion, etc.) are included via a simple two-body Morse-Stretch (MS) term,

$$U_{ij}^{\text{MS}}(R_{ij}) = D_0[e^{\gamma(1-R_{ij}/R_0} - 2e^{\gamma/2(1-R_{ij}/R_0)}]. \qquad (3)$$

The MS parameters for Si-O, O-O, and Si-Si, were optimized to describe the properties (density, cohesive energy,

TABLE I. Force field parameters for SiO_2.

(a) Morse stretch parameters [see Eq. (6)]			
	R_0 (Å)	D_0 (kcal/mol)	γ
O-O	3.7835	0.5363	10.4112
Si-Si	3.4103	0.2956	11.7139
Si-O	1.6148	45.9970	8.8022
(b) QEq parameters for O and Si (see Ref. [9])			
	χ (eV)	J (eV)	R (Å)
O	8.741	13.364	0.669
Si	4.168	6.974	1.176

 0031-9007/99/82(8)/1708(4)$15.00

elastic moduli, etc.) of α quartz and stishovite as representative fourfold and sixfold coordinated polymorphs. We refer to this as the MS-Q FF (MS plus charge). Table Ia gives the optimum parameters for D_0 (bond strength), R_0 (bond length), and γ (dimensionless force constant).

MS-Q describes well all fourfold and fivefold coordinated polymorphs of silica. Table S-I of the supplementary material compares the experimental structures with the results of Parrinello-Rahman-Nosè isothermal-isotension (NPT) [11–13] MD simulations at experimental temperatures for various silica polymorphs. The calculated charges for the various polymorphs are given in Table II, where we see that changes in the charges are significant. Coulomb interactions were evaluated using Ewald summation with real space cutoffs 5–8 Å and reciprocal space cutoffs 0.8–0.5 (1/Å). Morse interactions were truncated at $R = 9.0$ Å. The integration time step in all MD simulations was 1 fs.

With the MS-Q FF, the charges depend on the instantaneous geometry of the structure [we update the charges every 25 to 100 steps (0.025 to 0.1 ps)]. Thus, the charges readjust to the changes in atomic configuration. In addition, the charges depend intrinsically on the pressure and temperature, making MS-Q suitable for studying the phase transitions between the silica forms [quartz and coesite (both fourfold coordinated Si) have been observed to transform to stishovite at ~15 GPa in shock experiments [14,15]].

We consider pressure-induced phase transitions, in particular the dependence of transition pressure on temperature and pressure loading rate. In our simulations we used 576- to 640-atom 3D periodic models to describe α quartz, coesite, stishovite, and silica glass (perturbation of which will be detailed below).

In a continuous NPT MD simulation, we increased the pressure on the system by 1 GPa every ps. (We find similar behavior for loading rates of 0.25 and 0.05 GPa/ps; i.e., the transition pressure has a very weak dependence on the rate, 1 GPa higher for the lowest rate.) Figure 1(a) shows a sharp transition (at 15 to 20 GPa) from α quartz to stishovite (containing numerous defects), but the transition from glass to stishovite is quite gradual (17 to 100 GPa). Starting with α quarts, and using a 1 GPa/ps compression rate, we also did simulations at 500 to 1500 K. (Probably, the temperatures in shock experiments range from 1000 to 1500 K. However, we should note that these simulations do not represent simulation of shock experiments.) In Fig. 1(b), we see that the phase transition changes from 19.5 GPa (300 K) to 16.5 GPa (500 K), 15.5 GPa (1000 K), and 14.5 GPa for 1500 K. Experiments indicate a transition starting at about 14 GPa for 500 K [14], in reasonable agreement with our result of 16.5 GPa at 500 K. We also found that, if the parameters were biased to get better cristobalite structures, the phase transition from α quartz to stishovite again occurred, but at a higher pressure

TABLE II. Average QEq charges for the experimental structures of eight silica polymorphs and glass structures.

	No. of Molecules	Si	O
α quartz	3	1.318	−0.659
β quartz	3	1.293	−0.647
Stishovite	2	1.397	−0.699
β tridymite	4	1.217	−0.609
α cristobalite	4	1.281	−0.640
β cristobalite	8	1.216	−0.608
Keatite	12	1.290	−0.645
Coesite	16	1.339	−0.670
Glass[a]	216	1.318	−0.659
Glass[a]	200	1.328	−0.664

[a] Starting from β-cristobalite structure (cooling rate 100 K/4 ps).
[b] Starting from β-cristobalite structure(cooling rate 100 K/8 ps).
[c] Starting from random structure (cooling rate 100 K/4 ps).

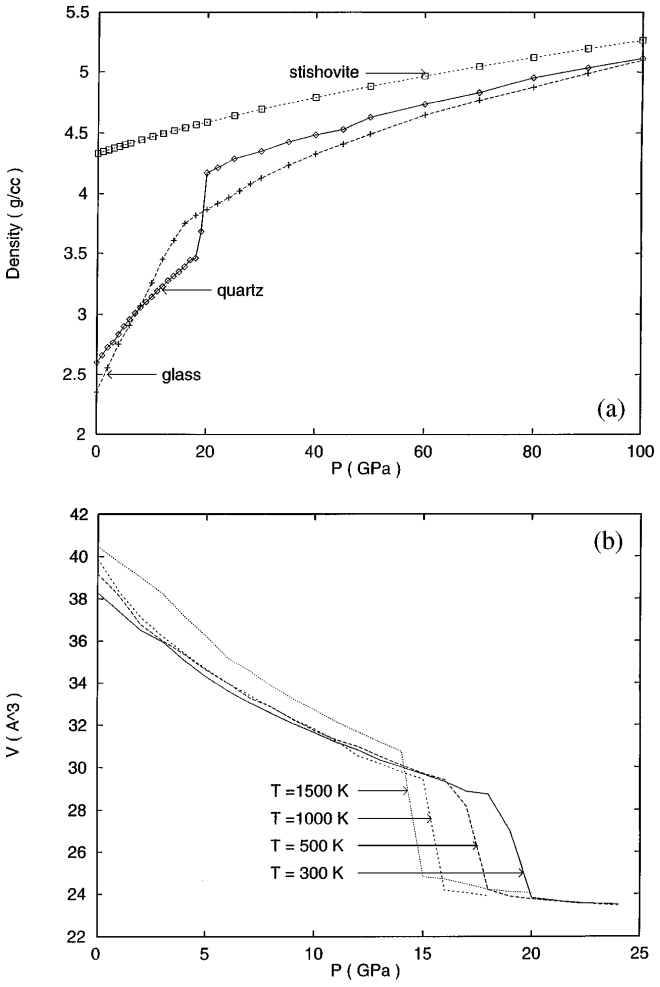

FIG. 1. (a) Equilibrium density per SiO_2 for α quartz, stishovite, and silica glass as a function of pressure from NPT MD using a fixed pressure loading rate of 1.0 GPa/ps. (b) Equilibrium volume per SiO_2, starting with α quartz for various temperatures ranging from 300 to 1500 K.

of 26 GPa at 300 K. We also performed a simulation on α quartz using fixed charges; the transition pressure dropped by 1 GPa, however, the final structure has 2% lower density.

To understand the origin of the difference in transformation for α quartz vs glass, we analyzed the average O-Si-O angle as a function of pressure. Figure 2(a) shows the average bond angles at the Si (over each 1 ps of dynamics) for α quartz. Here, we find a dramatic change between 15 and 20 GPa, where the average bond angle changes from nearly all tetrahedral (109.5°) at 15 GPa to mostly octahedral (90°) at 20 GPa. This indicates an abrupt reconstructive (nondiffusive) structural phase transformation for the crystal. In contrast for silica glass, Fig. 2(b) shows that the fivefold to sixfold coordinated local structures emerged slowly as the pressure increased from 20 to 120 GPa. Here the O-Si-O angle distribution changes appreciably between 20 and 30 GPa and continues to change significantly at higher pressures. This indicates a displacement phase transformation for the glass. Here the rearrangement requires diffusion. Even at 100 GPa, the percentage of sixfold coordinated atoms for silica glass is less than for the structures obtained from quartz. These results are consistent with the interpretation by Stolper and Ahrens [14] of the experiments [15].

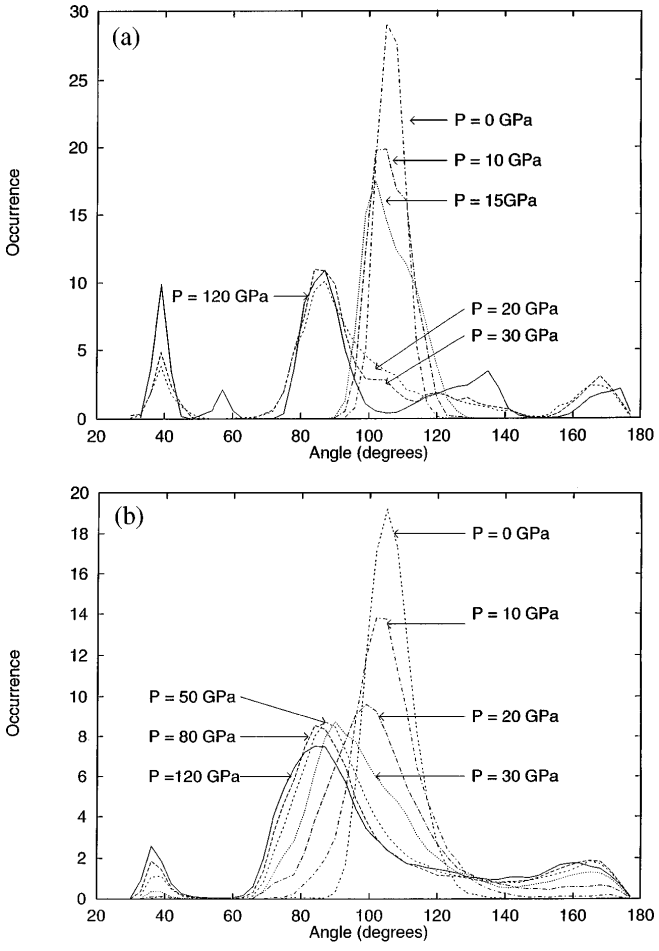

FIG. 2. The Si-centered angle distribution for a pressure loading of 1 GPa/ps at 300 K. (a) Starting with α-quartz crystal and (b) starting with silica glass.

We find that the α-quartz to stishovite transformation is not reversible at our time scales. Thus, relaxing the load from 100 GPa back to zero (at -1 GPa/ps) results in a structure with a density of 3.7 g/cm^3 at zero pressure. This is consistent with experimental observations of shock wave release isentropes [14,15].

To simulate the structural properties of silica glass, we prepared the sample in two ways: (a) We started with the crystalline form of β cristobalite (27 unit cells, leading to a supercell with 648 atoms) and annealed the structure at 4000 K with 40 ps of *NVT* dynamics. We then cooled the system slowly (4 ps per 100 K) using constant volume, constant temperature (*NVT*) dynamics until 1000 K. At 1000 K, we switched to NPT dynamics and continued cooling at the same rate. Finally, we performed 30 ps NPT dynamics at 300 K, leading to a final density of 2.32 g/cm^3. In a second simulation we cooled the systems more slowly (8 ps per 100 K) and found the final density, 2.33 g/cm^3. This indicates that slower cooling is unlikely to change the density. However, cooling at 2 ps/100 K leads to a final density of 2.35 g/cm, indicating that this is too fast. Thus, the 4 ps per 100 K cooling scheme seems adequate for predicting properties of silica glass. The final density 2.32–2.33 g/cm^3 from NPT simulations is 6% higher than experimental silica glass density at 2.20 g/cm^3 (b) A second simulation started with a randomly generated structure in a box of 200 Si and 400 O atoms (at a density of 2.20 cm^3). Using a similar quenching scheme (4 ps per 100 K) leads to a final density of 2.33 g/cm^3.

The most quantitative information about the structure of silica glass is from neutron diffraction. The fundamental quantity to be compared between experimental and theoretical results is the total correlation function for neutron scattering, $T(r) = 4\pi r\langle\rho(r)\rangle$, where $\rho(r)$ is the density function. $T(r)$ can be written in terms of neutron scattering lengths, b_X, and the radial distribution function, $G_{ij}(r)$,

$$T(r) = 4\pi r\rho_0 N_{\text{u.c.}}\left\{\sum_{i,j} f_i f_j b_i b_j G_{ij}(r)\right\}, \qquad (4)$$

where $N_{\text{u.c.}}$ is the number of atoms per unit of composition, f_X is the fraction of X-type atoms, and ρ_0 is the average density. Using $G_{ij}(r)$ [16], ρ_0 obtained from the 30-ps-long NPT MD simulations of three glass structures at 300 K and $b_{\text{O}} = 5.805$ fm, $b_{\text{Si}} = 4.1491$ fm, we calculated $T(r)$. Figure 3 shows that the calculated total correlation functions are in good agreement with a neutron scattering experiment [17] for the first two peaks (up to 3 Å) and reasonably good for the next three peaks (up to 5.5 Å). The simulations do not show the small peaks

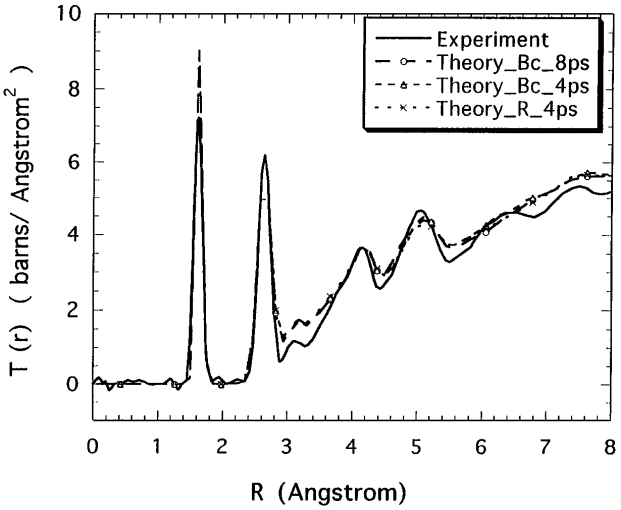

FIG. 3. The total correlation function $T(r)$ from NPT MD simulations for two samples of silica glass at $T = 300$ K: (i) Glass obtained from the β-cristobalite (648 atoms/cell) melts at both the 100 K/8 ps and 100 K/4 ps cooling rates; (ii) glass obtained from random structure (600 atoms/cell) melts at the 100 K/4 ps cooling rate. Calculations are carried out using 0.12 Å resolution. The symbols help distinguish the lines. The experimental neutron scattering data is from Ref. [17].

observed at 6.3 and 7.5 Å. Thus, the simulations account for the Si-O and O-O spacings, indicating that three-body terms are *not* required to describe the open Si-O-Si bond angles. The discrepancy for >6 Å might be due to the periodic supercells or the fast time scale for annealing.

In summary, we developed the MS-Q-type FF for describing phase transitions of materials and have applied it to SiO_2. We find that MS-Q describes well the fourfold and sixfold coordinated crystal systems (such as quartz and stishovite), the formation of silica glass, and the pressure-induced phase transitions from quartz or silica glass to the stishovitelike dense phase.

We thank Professor Tom Ahrens for helpful discussions. This research was initiated with support from Owens Corning and continued with support from DOE-ASCI. The facilities of the MSC are also supported by grants from NSF (CHE 95-22179), ARO/DURIP (Kiserow), BP Chemical, ARO-MURI (Kiserow), Exxon, Seiko-Epson, Asahi Chemical, Beckman Institute, Chevron Petroleum Technology Co., Chevron Chemical Co., NASA/Ames, NASA/JPL, ONR, Avery Dennison, and Chevron Research Technology Co.

Supplementary material available:—The comparisons of experimental structures and the results of NPT simulations at experimental temperatures for various silica polymorphs were shown in Ref. [18] (Table SI).

*Electronic address: erd@wag.caltech.edu
†Electronic address: tahir@wag.caltech.edu
‡Electronic address: wag@wag.caltech.edu

[1] R. E. Cohen, I. I. Mazin, and D. G. Isaac, Science **275**, 654 (1997).
[2] L. Strixrude, R. E. Cohen, R. Yu, and H. Krauker, Am. Mineral. **81**, 1293 (1996).
[3] F. Liu, S. H. Garofalini, D. Kingsmith, and D. Vanderbilt, Phys. Rev. B **49**, 12 528 (1994).
[4] L. V. Woodcock, C. A. Angell, and P. Cheeseman, J. Chem. Phys. **65**, 1565 (1976).
[5] B. P. Fueston and S. H. Garofalini, J. Chem. Phys. **89**, 5818 (1988).
[6] S. Tsuneyuki, H. Aoki, M. Tsukada, and Y. Matsui, Phys. Rev. Lett. **61**, 869 (1988).
[7] H. Ogawa and Y. Waseda, Sci. Rep. Tohoku Univ. Ser. A. Phys. Chem. Metall. **36**, 20 (1991).
[8] (a) S. L. Mayo, B. D. Olafson, and W. A. Goddard III, J. Phys. Chem. **94**, 8897 (1990); (b) A. K. Rappé, C. J. Casewitz, K. S. Colwell, W. A. Goddard III, and W. M. Skiff, J. Am. Chem. Soc. **114**, 10 024 (1992).
[9] A. K. Rappé and W. A. Goddard III, J. Phys. Chem. **95**, 3358 (1991).
[10] C. F. Fan and T. Çağin, J. Chem. Phys. **103**, 9053 (1995); E. Demiralp and W. A. Goddard III, J. Phys. Chem. **98**, 9781 (1994).
[11] M. Parrinello and A. Rahman, Phys. Rev. Lett. **45**, 1196 (1980); M. Parrinello and A. Rahman, J. Appl. Phys. **52**, 7182 (1981).
[12] S. Nosé, Mol. Phys. **52**, 255 (1984); S. Nosé, J. Chem. Phys. **81**, 511 (1984).
[13] (a) K-T. Lim, S. Brunett, M. Iotov, R. B. McClurg, N. Vaidehi, S. Dasgupta, S. Taylor, and W. A. Goddard III, J. Comput. Chem. **18**, 501 (1997). (b) In the simulations, we used a dynamics step of 0.001 ps, an NPT dynamics mass prefactor of 0.125, and a Nosé relaxation time constant of 0.25 ps [see (c) and (d)] (c) T. Çağin, N. Karasawa, S. Dasgupta, and W. A. Goddard III, Mater. Res. Soc. Symp. Proc. **278**, 61 (1992); (d) T. Çağin, W. A. Goddard III, and M. L. Ary, Comput. Polymer Sci. **1**, 241 (1991).
[14] E. M. Stolper and T. J. Ahrens, Geophys. Res. Lett. **14**, 1231 (1987).
[15] J. W. Swegle, J. Appl. Phys. **68**, 1563 (1990), and references therein.
[16] The experimental real space resolution $\Delta r = 0.12$ Å was used for the $G_{ij}(r)$ calculations.
[17] A. C. Wright, J. Non-Cryst. Solids **179**, 84 (1994).
[18] See AIP Document No. E-PAPS: E-PRLTA-82-020908 for lattice constants for silica polymorphs from the experiment and NPT simulations using MS-Q. E-PAPS document files may be retrieved free of charge from our FTP server (http://www.aip.org/epaps/epaps.html) or from ftp.aip.org in the directory /epaps/. For further information, email: paps@aip.org; or fax: 516-576-2223.